Project no. **316488**

Project Acronym: KESTCELLS

Project title: Training for sustainable low cost PV technologies: development of kesterite based efficient solar cells.

Industry-Academia Partnerships and Pathways

Start date of project: 01/09/2012

Duration: 48 months

Project coordinator: Dr. Edgardo Saucedo

Project coordinator organization name: IREC

Project website address: www.kestcells.eu

Deliverable D5.2
Complete modeling of the optimized kesterite solar cells

Delivery date: Month 46 (June 2016)

Dissemination Level:	PU
PU	Public
PP	Restricted to other programme participants (including the Commission Services)
RE	Restricted to a group specified by the consortium (including the Commission Services)
CO	Confidential, only for members of the consortium (including the Commission Services)

Document details:	
Workpackage	5: Modelling & design
Partners	AMU
Authors	Dario Cozza
Document ID	D5.2
Release Date	

1 General introduction

Workpackage 5 (WP5) is concerned with the modelling and simulation of kesterite based solar cells with the aim of designing optimal solar cells configurations and to improve the understanding of the physical mechanisms affecting the device figures of merits (V_{oc}, J_{sc}, FF, μ). Kesterite based solar cells are an interesting alternative to other thin film photovoltaic technologies due to promising performances combined to earth-abundant elements composition. The most efficient kesterite solar cells to-date with η=12.6% have been fabricated using the solid solution $Cu_2ZnSn(S,Se)_4$ (CZTSSe), which exhibits an intermediate band gap (Eg) relative to the pure selenide $Cu_2ZnSnSe_4$ (CZTSe, Eg ≈ 1.0 eV) and sulfide Cu_2ZnSnS_4 (CZTS, Eg ≈ 1.5 eV) [1]. Despite a rapid progress achieved by different groups in a short time, many aspects are not well understood yet in terms of material properties and working mechanisms of the device. Optical and electrical modeling and simulations can be a powerful tool to overcome this gap. In this deliverable we report the advancements achieved by the WP5 in developing new 1D and 2D numerical models of Kesterite solar cells and their applications for optimizing the design and to analyze the limiting factors for the performances of these devices (especially V_{OC} and FF).

In section 2.1 we will deal with the role of the $MoSe_2$ interfacial layer in CZTSe solar cells: we will propose the values of material parameters required for the simulations of this layer and we will provide a picture of the simulated band diagram of the full CZTSe solar cell including $MoSe_2$ and Molybdenum (Mo) at the back contact.

In section 2.2 we will discuss a design optimization in terms of optimal thickness of the TCO and buffer layers for the CZTSe solar cells obtained by multiple TMM optical simulations.

In section 3 we will deal with the grain boundaries (GBs) of kesterite. We will perform a comprehensive theoretical study of different possible physical mechanisms that could be present at the GBs, according to the information found in literature, and we will try to correlate the theoretical results with some experimental observations. More precisely we want to investigate possible links between the well-known V_{OC} deficit that still characterizes kesterite solar cells and the electrical activity of the grain boundaries.

2 1D simulations of the CZTSe cell Back Contact and Design Optimizations

Even though 2D simulations are typically more accurate than 1D simulations, the counterpart of this benefit is the need of a higher number of required material parameters, higher level of complexity for the definition of the models and a higher computational cost than the 1D case. The limit of the 1D simulation is that it cannot take into account some of the morphological features of the materials and the non-uniformities of the properties along the horizontal direction. It is a matter of trade-off, but 1D or 2D modeling would result in a better option depending on the specific problem to be studied. In the following paragraphs we will first discuss a work devoted to the investigation of the effects of the back contact of a CZTSe solar cell. In a second part, we will deal with the optical optimization of an experimental solar cell from IREC, with the aim of improving its design. For both these cases we employed 1D modeling strategies because we did not expect that the use of 2D models could produce very different results such to motivate more complex implementations. The electrical simulations were performed with the software SCAPS [2]. A default value of external shunt resistance equal to 10^3 Ω•cm^2 was also considered in these models.

2.1 Modeling and simulations of the CZTSe back contact

The metal back contact that is commonly used for kesterite solar cells is Molybdenum (Mo). Between the Molybdenum and the kesterite layers, a $Mo(S,Se)_2$ interfacial layer is also present: the formation of this layer is a result of the kesterite post-deposition annealing and the control of its growth is a matter of study [3]. In literature there is an open debate about the effects of the $Mo(S,Se)_2$ interfacial layers and their actual role in affecting the performances of kesterite solar cells. Moreover a majority of papers in literature dealing with modeling of CIGS/Kesterite solar cells completely neglect the effects of both the $Mo(S,Se)_2$ and the Molybdenum by assuming

the flat band condition between the absorber and the back contact [3]. Focusing on a pure selenium CZTSe absorber, we performed 1D simulations of three different structures (A,B and C), in order to study the evolution of the cell performances from the ideal case (A) to the more realistic case (C). The three considered structures are illustrated in Fig. 1. A is a ZnO/CdS/CZTSe structure with flat band condition at the back contact (ideal case). The second structure (B) is $MoSe_2$-free similarly to A, but with work function (W_f) values at the back contact that are inside the realistic range of values reported in literature for the Molybdenum metal (see Table I). The third structure (C) includes at the same time a realistic Mo W_f value and a 100 nm thick p-type $MoSe_2$ layer between the CZTSe layer and the Mo contact.

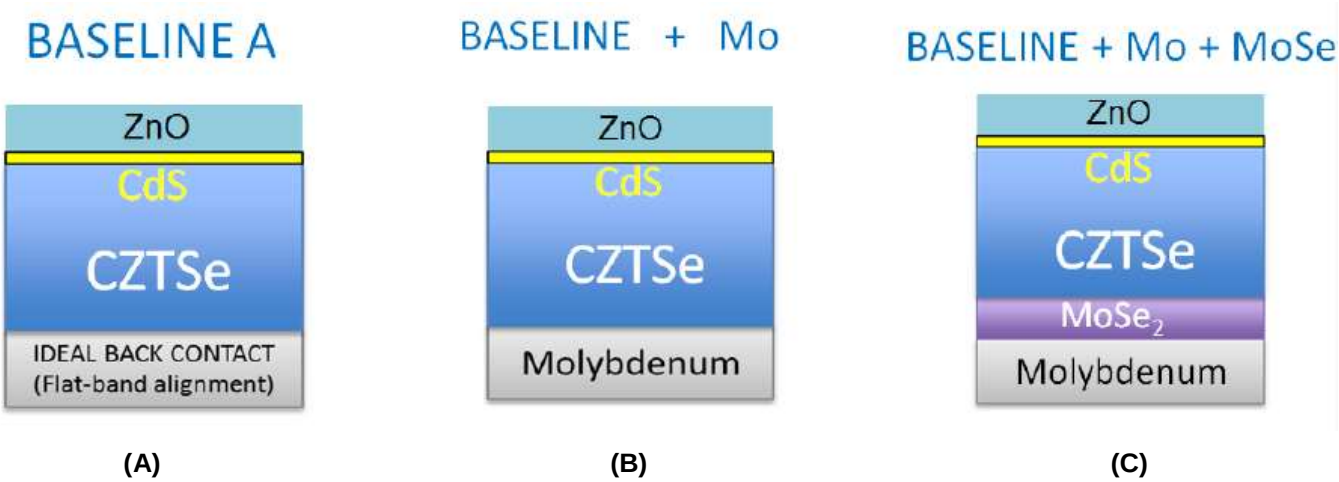

Figure 1: Schemes of the three types of structures that will be simulated in the following sections. (A) an ideal structure with flat-band alignment at the back contact; (B) a MoSe2-free structure with realistic values of Mo Wf at the back contact; (C) a complete structure including both Mo and MoSe2.

The material parameters (electrical and optical) for the ZnO/CdS/CZTSe layers are reported in Cozza et al. (2016) [3]. Since many material parameters of $MoSe_2$ are not clearly understood yet, we modeled this layer with the same properties as the CZTSe layer but different band gap (E_g), electron affinity (χ), and electron/hole mobility (μ_n, μ_p) (see Table II) . The indirect E_g of $MoSe_2$ is often reported to be around 1.1 eV and high values of carriers mobility are expected if this layer is oriented with the c-axis parallel to the substrate [3]. We are not aware of any measured values of electron affinity but a possible value equal to 4.14 eV (bulk $MoSe_2$) was calculated by Kang through ab-initio simulation methods [4].

TABLE I
MOLYBDENUM WORK FUNCTIONS

Wf_{Mo}	MAX	AVERAGE	MIN
eV	4.95 (110)	4.6 (Poly)	4.36 (112)

Molybdenum W_f (Wf_{Mo}) as reported in Ref.3. In brackets the crystal lattice orientation. Polycrystalline Mo W_f has an average value in between the (110) and the (112) case.

TABLE II
$MoSe_2$ INPUT ELECTRICAL PARAMETERS

Material	Eg (eV)	χ (eV)	μ_p, μ_n (cm^2/Vs)
$MoSe_2$	1.1	4.14	25,100

E_g, χ, μ_p and μ_n used as input parameters for the simulation of the $MoSe_2$ layer (from Ref.3).

In Fig. 2(a-b) we can see the simulated band diagram relative to the structures B and C (solid lines) compared to the ideal structure A (dashed lines). In Fig. 2(a) we observe that, decreasing the W_f of the back contact from the

flat band condition (A) to 4.9 eV (B) in a $MoSe_2$-free structure, the CB and VB of the CZTSe layer are both bended downwards at the back contact side. This condition induces a potential barrier in the VB, which hinders the extraction of holes, and an energetically favorable path for electrons towards the back contact in the CB, which increases the recombination near the CZTSe-Mo interface. The energy barrier for holes, considering W_f = 4.9 eV (B), is equal to 0.55 eV and it is big enough to completely block the forward current of the structure B in the dark condition as it can be seen in Fig.3 (green dashed line).

The band diagrams of structure C and A are illustrated in Fig. 2(b) and the corresponding J-V curves are visible in Fig.3. From the analysis of the J-V curves we observe that the strong V_{OC} loss induced by the decreasing of the back contact W_f (from structure A to structure B) is almost completely restored moving from B to C. The anomalous crossover between illuminated and dark J-V curves existing in the structure B is not present in the structure C (see Fig.3). Moreover structure C has the best J_{SC} among the three cases (+1.12 mA/cm^2 with respect to A). From the analysis of the band diagram of structure C we can notice that this structure has two advantages compared to the structure B (see Fig.2(a-b)):

- the $MoSe_2$ induces an energy barrier of about 0.4 eV in the CB at the CZTSe-$MoSe_2$ interface, that keeps the electrons away from the Mo contact;
- it decreases the effective barrier for holes in the VB, splitting the big 0.55 eV barrier, present in structure B, into two smaller barriers of 0.29 eV for the CZTSe-$MoSe_2$ interface and 0.26 eV for the $MoSe_2$-Mo interface.

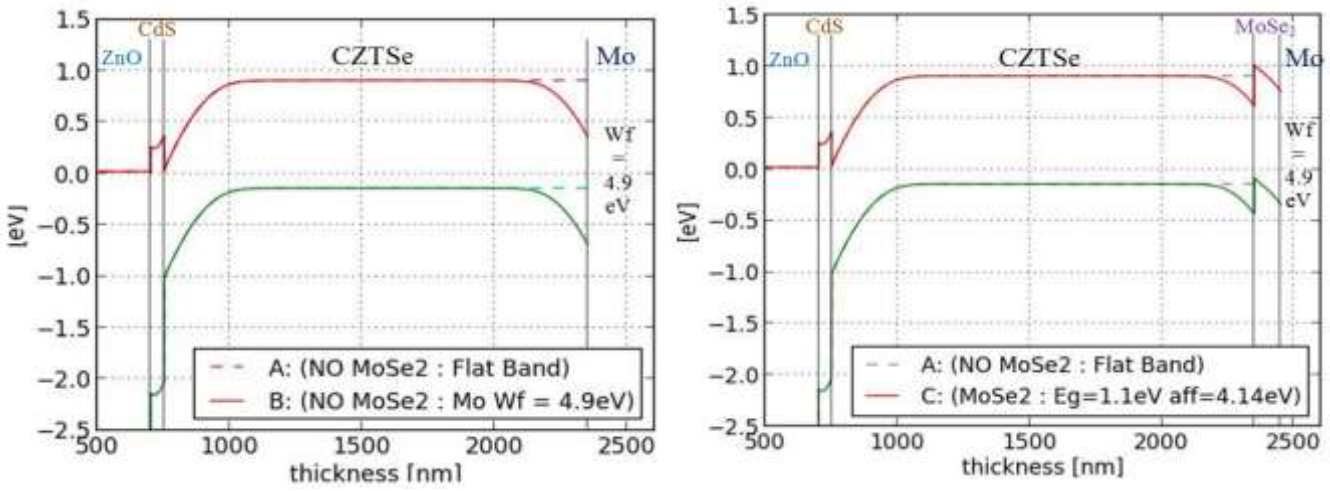

(a) (b)

Figure 2: Simulated Band Diagrams in dark condition of (a) structures A and B and (b) of structures A and C. Conduction Band in red and Valence Band in green.

An experimental evidence of the validity of our model (structure C) is given by the work by López-Marino [5]. He reports CZTSe solar cells with different $MoSe_2$ thicknesses (under 120 nm) and he demonstrates that the device performances (especially V_{OC}) are significantly lowered by decreasing the thickness of this interfacial layer under a threshold of about 50nm. In order to compare these experimental results to our model we performed J-V simulations (illuminated condition) of the structure C considering a variable thickness of the $MoSe_2$ layer from 170 to 0 nm. In Fig.4 we can see that the theoretical trends (simulations) in terms of V_{OC} and η losses are comparable to the results obtained by López-Marino [5].

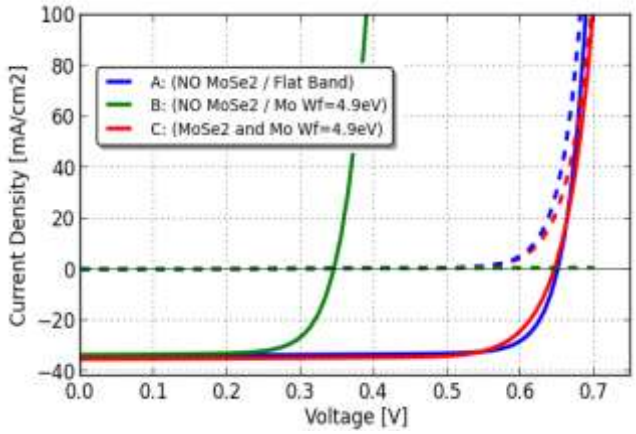

Figure 3: Simulated J-V curves of structures A, B and C: dark (dashed lines) and illuminated (solid lines) condition.

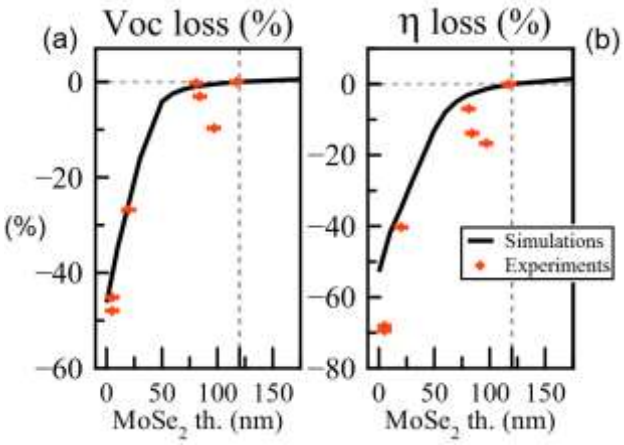

Figure 4: (a) V_{OC} losses and (b) η losses (normalized values expressed in percentage) as a function of the thicknesses of the $MoSe_2$ layer. The thicknesses of the experimental values (from López-Marino [5]) were measured by Scanning Electron Microscopy (SEM) and their uncertainty is ±5nm.

2.2 Optical optimizations

In this section we will apply the previous model for an optimization of the thickness of the top layers (the buffer and the TCO) that can maximize the J_{SC} of the device by maximizing the transmission of light into the absorber. The baseline for this section presents a 440nm TCO layer (ITO+iZnO), a 50nm CdS buffer layer, a 1.8 μm thick CZTSe layer, a 380nm thick MoSe2 layer, similarly as an experimental cell from IREC institute reported in Neuschitzer et al. [6]. The Mo contact was modeled with a Wf = 4.95eV. More details about this model were described in previous works [7].

By mean of TMM optical simulations we quantitatively estimated the percentage of photons that are reflected and lost from the top surface of the baseline and the number of photons that are absorbed by the CZTSe layer. The percentage of reflected photons per unit area per second was computed in the spectral range 300-1300 nm as follow:

$$R_{\%} = \int_{300nm}^{1300nm} N_{ph-AM1.5}(\lambda) R(\lambda) d\lambda \Big/ \int_{300nm}^{1300nm} N_{ph-AM1.5}(\lambda) d\lambda \quad [\%] \qquad (1)$$

where R(λ) is the spectral reflectance computed by TMM and $N_{ph\text{-}AM1.5}$ is the solar spectral irradiance AM1.5. Similarly, the generated photocurrent inside the CZTSe layer (J_{ph}) was computed considering the spectral range 300-1300nm as follow:

$$J_{ph} = q \int_{300nm}^{1300nm} N_{ph-AM1.5}(\lambda) A_{CZTSe}(\lambda) d\lambda \quad \left[\mathrm{mA/cm^2}\right] \qquad (2)$$

where q is the electron charge and $A_{CZTSe}(\lambda)$ is the spectral absorption of photons inside the CZTSe . J_{ph} can be considered as an upper bound for the final short circuit current J_{SC} of the device [8].

Multiple TMM simulations were performed by varying the thickness of CdS (buffer) between 0-100 nm and the thickness of ITO/ZnO (TCO) between 0-600 nm. The results of these multiple optical simulations are illustrated in Fig.5. On the left we can see the simulations related to the standard structure without Anti Reflective (AR) coating.

On the right we can see the simulations of a structure including also a 110 nm thick MgF_2 AR coating on the top of the TCO layer. The thickness of the MgF_2 was chosen similar to other cases from literature [8]. The point labelled A in the figures 5(a-b) represents the baseline configuration, explained above. From the analysis of Fig. 5(a) (bottom) we can see the existence of two regions where the photocurrent is maximized: one is the region surrounding the point B (TCO thickness equal to 300 nm) and the other region is at very low values of the TCO layer thickness (< 100 nm).

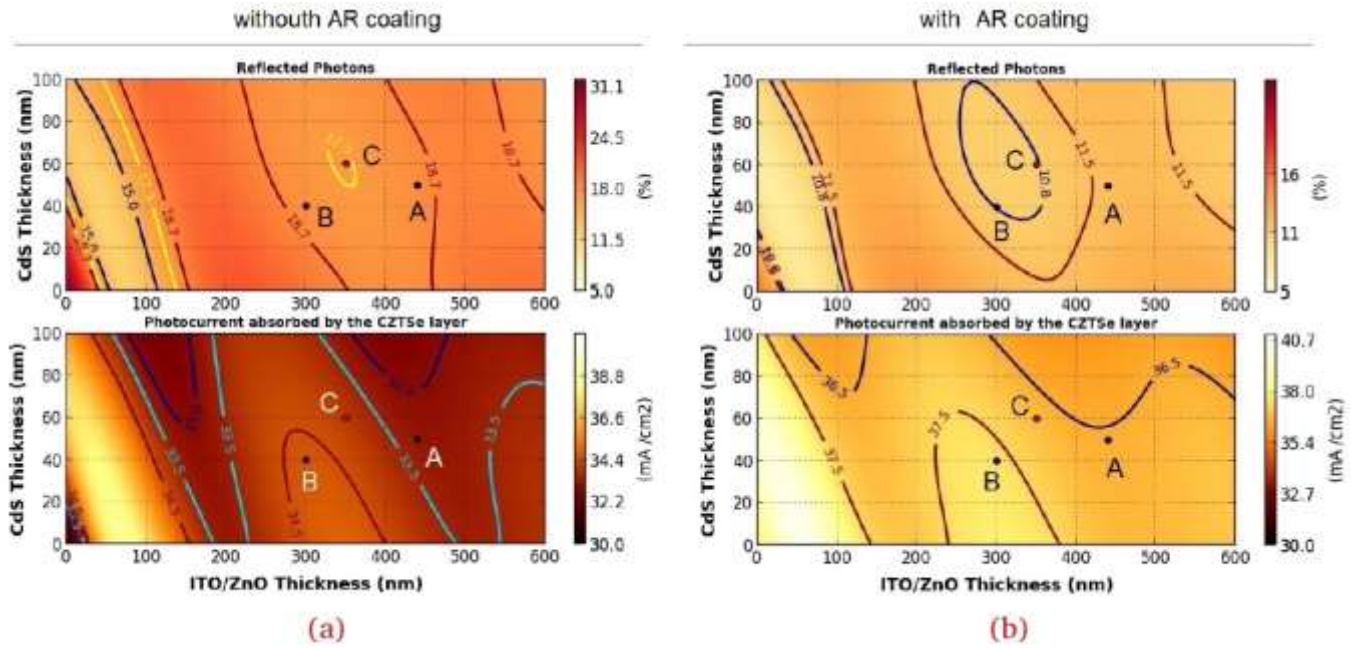

Figure 5: TMM Simulation of the percentage of reflected photons $R_{\%}$ (top) and the generated photocurrent (bottom) of a CZTSe solar cell as a function of the CdS and ITO/ZnO layers thickness. The point A corresponds to the reference cell used as baseline. The point B is a possible optimal point maximizing the photocurrent. (a) Simulation performed without AR coating; (b) Simulation performed including a 110 nm thick MgF2 layer (AR coating) on the top of the TCO.

Considering these two regions the J_{ph} is bigger if the thickness of CdS is as small as possible. In the graphs we also plotted a point called C which is in a minimum of reflection (Fig.5(a), above): comparing the points B and C we want to point out the fact that the points where J_{ph} is maximized do not necessarily correspond to points of minimal reflection $R_{\%}$. The point B represents our proposed optimized point, with a CdS thickness = 40 nm and a TCO thickness = 300 nm. We did not consider the area of the graph with a very thin ITO/ZnO because, with this configuration, technological issues (pinholes) could rise during the fabrication of the cell.

3 2D modeling of grain boundaries and influence on the performances of CZTSe solar cells.

A 2D model was developed in order to simulate the grain boundaries (GBs) that are present in the polycrystalline CZTSe layer. For this work we employed the software Silvaco®. According to previous works on two-dimensional modeling of CIGS solar cells, three main mechanisms could be present at the grain boundaries of these thin film polycrystalline materials [9-11]:

(i) a high recombination velocity SR;

(ii) charged trap states that can induce a local potential bending;

(iii) a different band gap if a different material phase is actually dominant at the GB.

These works investigated the impact of the combination of these three factors on the device performances as well as the role of local potential bending and/or band gap shifts to attenuate the carriers recombination at the GBs when a high value of SR is considered.

We are aware of only one paper applying similar concepts to perform two-dimensional simulations on CZTSe solar cells [12]: in this work Kanevce modeled the GBs as regions with higher recombination and a different band gap with respect to the intra-grains (IGs). In this paper they mentioned other works that claimed the possible accumulation of Cu-rich kesterite and ternary phases in the vicinity of the grain boundaries: these phases are expected to have a smaller band gap compared to the intragrains (IGs) with a difference ΔEg = Eg(GB)-Eg(IG) up to -0.4 eV [12]. Kanevce found that high surface recombination (SRV) at the GBs is detrimental for V_{OC}, that a positive ΔEg could partially restore the V_{OC} loss due to the SRV and that a negative ΔEg can worsen the V_{OC} loss because of a resulting higher recombination rate at the GBs, even for low values of SRV.

From the experimental point of view KPFM measurements carried out on Kesterite solar cells revealed a higher positive surface potential at the GBs compared to the intra-grains [13]. In our work we consider five different physical mechanisms that could exist at the GBs and we analyze both the effect of these mechanisms on the performances (V_{OC}, J_{SC}, FF, η) and their effect in terms of induced potential difference ($\Delta V_{GB-IG} = V_{GB}-V_{IG}$) along the horizontal direction Y. More details about the computation of ΔV_{GB-IG} are reported in previous works [7].

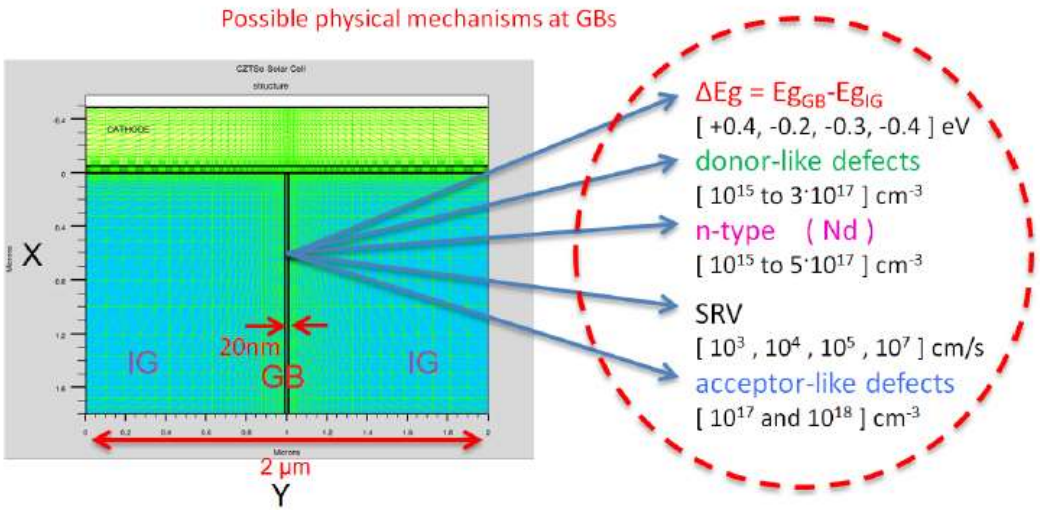

Figure 6: Representation of the 2D model implemented in Silvaco® and list of the physical mechanisms that have been implemented in the GB.

3.1 2D Baseline model

In Fig.6 we can see an example of the scheme of our 2D model. It is a CZTSe cell structure including the CZTSe absorber (1.8 µm), CdS buffer (50 nm) and ZnO window (440 nm) layers and the flat band condition at the back contact. Here we did not implement the advanced modeling for the back contact (described in section 2.1) in order to decouple the effect of GBs from the possible interaction with the Mo and MoSe2 layers. Optical simulations for the 2D model were performed using the TMM method. In Fig. 6 we can also see that the thickness of the layers of this cell is considered along the X-axis and the total width along the Y-axis is always equal to 2µm.

The GB is modeled as a stripe of the same thickness of the kesterite layer and a width equal to 20nm. In Fig.6 (on the right) we also summarize the range of values for the different physical mechanisms that will be

implemented in the GB region. The mesh of the 2D structure is characterized by a higher number of nodes in the vicinity of the interfaces between different materials and less nodes elsewhere (in this case we have 2703 nodes and 5200 triangles): this mesh strategy is the one that maximizes the accuracy and minimizes the simulation time.

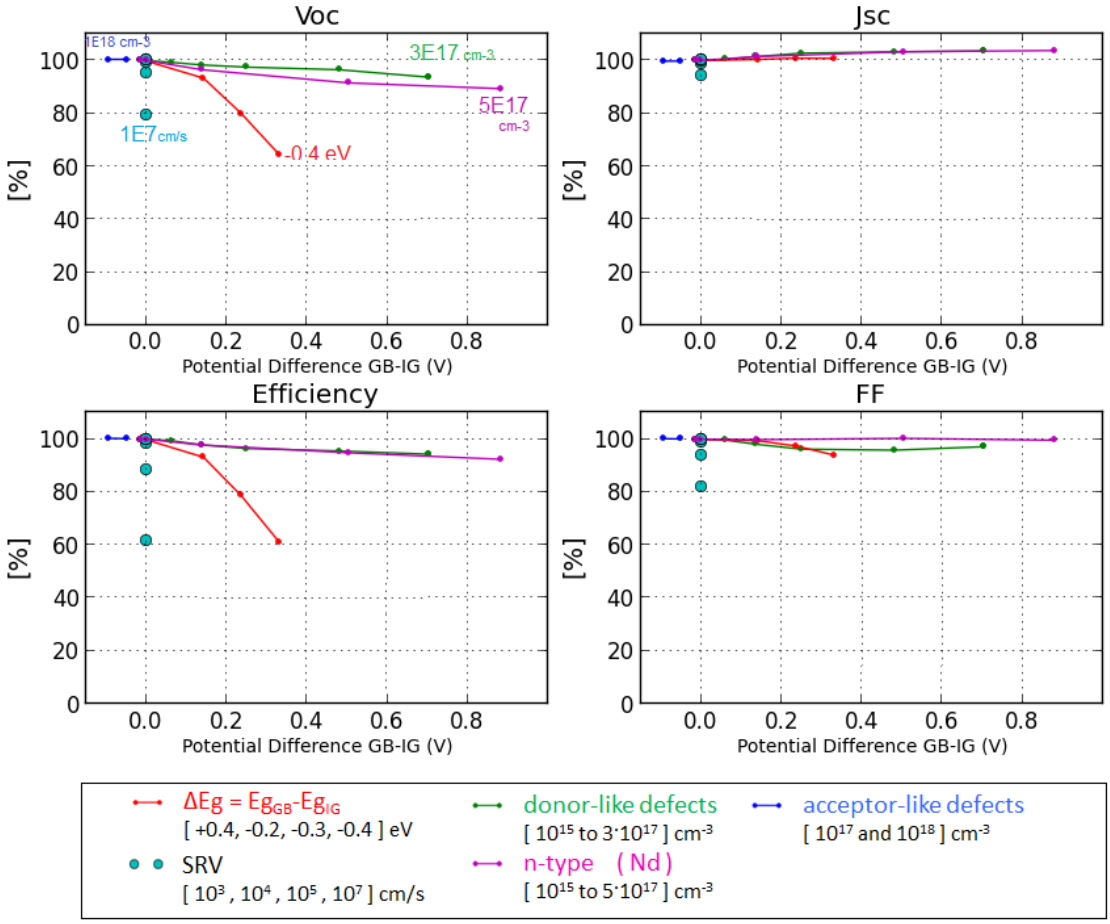

Figure 7: Device performances as a function of the simulated potential difference between GBs and IGs of CZTSe solar cells (ΔV_{GB-IG}). All the values are normalized with respect to the corresponding parameters of a GB-free structure.

3.2 Results

In Fig.7 we can see the effects that the different physical mechanisms can produce: the SRV alone only produces performance losses (no potential difference ΔV_{GB-IG}), especially V_{OC} and FF, but also J_{SC} (none of the other mechanisms can produce J_{SC} losses.). The implementation of a small band gap phase ($\Delta Eg < 0$, as seen in Fig. 7) can produce significant performance losses in terms of V_{OC} and moderate losses in terms of FF. $\Delta Eg < 0$ can also induce positive ΔV_{GB-IG} potentials up to more than 0.3V.

The cases of donor-like defects and n-type phases have a similar behavior in terms of efficiency and J_{SC}: the donor-like defects produce more losses in terms of FF and the n-type phases are more detrimental for the V_{OC}. Overall their impact on the performances is moderate and their impact in the ΔV_{GB-IG} is strong (up to 0.7-0.9 V) especially if their concentration is bigger than the doping of the main kesterite phase in the IGs. The implementation of acceptor-like phases seems to be neutral because they do not produce any performance losses and they produce very limited negative potentials ΔV_{GB-IG} also with very high traps concentrations (10^{18} cm^{-3}) that

are probably unrealistic. The case of ΔEg > 0 (ΔEg = 0.4 eV) does not produce any performance losses and it induces very limited negative ΔV_{GB-IG} potentials. Summarizing this analysis we observed the following trends:

- SRV and ΔEg < 0 are the mechanisms that produce the bigger losses, especially for the V_{OC};
- donor-like defects and n-type phases can induce big positive ΔV_{GB-IG} potentials but limited performance losses;
- ΔEg < 0 produces also positive ΔV_{GB-IG} potentials but smaller than the donor-like defects and the n-type phases;
- ΔEg > 0 and acceptor-like defects are quite neutrals.

4 Conclusions

The objective of this deliverable was to report the 1D and 2D numerical models of Kesterite solar cells developed by the WP5 and their applications for optimizing the design of the device and to improve the understanding of the physical mechanisms that limit some of the performances of this technology (V_{OC} and FF).

We improved the 1D model of the CZTSe solar cell (reported in the previous deliverable D5.1) by including the **Mo back contact and the $MoSe_2$** interfacial layer, proposing the values of material parameters required for simulations (see section 2.1). We could compute a complete picture of the **band diagram of the CZTSe solar cell including MoSe**2 **and the Mo back contact**. We could then provide a theoretical explanation of **the role of Mo and MoSe**2 **in affecting the performances of the solar cell** from an energetic point of view (role of the energy barriers between CZTSe/$MoSe_2$ and $MoSe_2$/Mo).

In section 2.2 we discussed a design optimization, in terms of **thickness of the TCO and buffer layers**, that can maximize the J_{SC} of the device. Winkler et al. previously performed similar optical simulations that highlighted the existence of optimal CdS-TCO thicknesses that maximize the photo-current of the device [8] : they proposed an optimal combination of 25 nm for CdS and 50 nm for the TCO. Since these very thin values could be difficult to be obtained in practical implementations we showed that a second *optimal region* exists for TCO thickness values between 250 and 350 nm and CdS thickness equal or lower than 50nm.

Finally in section 3 we introduced **2D models of CZTSe solar cells including vertical grain boundaries** in the absorber and we simulated several possible physical mechanisms that could be present inside the GBs. From an experimental point of view, positive potentials were previously reported in the vicinity of the CZTSe GBs (ΔV_{GB-IG} measured by KPFM). The results of our 2D simulations highlighted that some of the physical mechanisms implemented in the GBs can actually generate positive potentials comparable to the ones reported in literature. At the same time some of these physical mechanisms can also affect the performances of the device: we found that realistic trends, both in terms of performance losses (especially V_{OC}) and in terms of ΔV_{GB-IG} can be obtained implementing the GBs as material phases with small Eg (lower than the one of CZTSe) and with significant concentrations of donor-like defects in the GBs.

5 Acknowledgements

This research was supported by the Framework 7 program under the project KESTCELLS (FP7-PEOPLE-2012-ITN316488).

6 References

1. D. Cozza. "Modeling and physical studies of kesterite solar cells," PhD dissertation, Aix Marseille University, (2016).

2. Burgelman, M., Nollet, P., and Degrave, S., “Modelling polycrystalline semiconductor solar cells” Thin Solid Films 361-362, 527–532, 2000.
3. D. Cozza, C. M. Ruiz, D. Duché, J.J. Simon and L. Escoubas, “Modeling the back contact of $Cu_2ZnSnSe_4$ solar cells,” IEEE Journal of Photovoltaics, 2016, In press.
4. J. Kang, S. Tongay, J. Zhou, J. Li, and J. Wu, “Band offsets and heterostructures of two-dimensional semiconductors” *Appl. Phys. Lett.*, vol. 102, issue 1, pp. 22–25, 2013.
5. S.Lopez-Marino, “New processing approaches for $Cu_2ZnSnSe_4$-based solar cells”, Ph.D. thesis, Universitat Politècnica de Catalunya, Spain, 2016.
6. M. Neuschitzer, Y. Sanchez, S. Lopez-Marino, H. Xie, A. Fairbrother, M. Placidi, S. Haass, V. Izquierdo-Roca, A. Perez-Rodriguez, and E. Saucedo, "Optimization of CdS buffer layer for high-performance $Cu_2ZnSnSe_4$ solar cells and the effects of light soaking: elimination of crossover and red kink," Prog. Photovoltaics Res. Appl. **23**(11), 1660–1667 (2015).
7. D. Cozza, C. M. Ruiz, D. Duché, M. Neuschitzer, E. Saucedo, J. J. Simon, and L. Escoubas, "1D and 2D numerical simulations of $Cu_2ZnSnSe_4$ solar cells," in *Photovoltaic Specialist Conference (PVSC), 2015 IEEE 42nd* (2015), pp. 1–4.
8. Winkler, M. T., Wang, W., Gunawan, O., Hovel, H. J., Todorov, T. K., & Mitzi, D. B. Optical designs that improve the efficiency of Cu2ZnSn(S,Se)4 solar cells. Energy & Environmental Science. 2014.
9. W. K. Metzger and M. Gloeckler. “The impact of charged grain boundaries on thin-film solar cells and characterization”. In: *Journal of Applied Physics* 98.6 (2005), p. 063701. DOI: 10.1063/1.2042530
10. E.S. Mungan, Xufeng Wang, and M.A. Alam. “Modeling the Effects of Na Incorporation on CIGS Solar Cells”. In: *Photovoltaics, IEEE Journal of* 3.1 (2013), pp. 451–456.
11. C. Leendertz et al. “Evaluation of Kelvin probe force microscopy for imaging grain boundaries in chalcopyrite thin films”. In: *Applied Physics Letters* 89.11 (2006), p. 113120. DOI: 10.1063/1.2354474
12. Ana Kanevce, Ingrid Repins, and Su-Huai Wei. “Impact of bulk properties and local secondary phases on the Cu2(Zn,Sn)Se4 solar cells open-circuit voltage”. In: *Solar Energy Materials and Solar Cells* 133 (Feb. 2015), pp. 119–125. DOI: 10.1016/j.solmat.2014. 10.042.
13. Joel B Li, Vardaan Chawla, and Bruce M Clemens. “Investigating the role of grain boundaries in CZTS and CZTSSe thin film solar cells with scanning probe microscopy.” In: Advanced materials (Deerfield Beach, Fla.) 24.6 (Feb. 2012), pp. 720–3. DOI: 10.1002/adma.201103470